Journal of Magnetic Resonance **141,** 286–290 (1999)
Article ID jmre.1999.1923, available online at http://www.idealibrary.com on IDEAL®

In Vivo Triple Quantum Filtered Twisted Projection Sodium MRI of Human Articular Cartilage

Arijitt Borthakur, Ileana Hancu,* Fernando E. Boada,† Gary X. Shen,† Erik M. Shapiro,‡ and Ravinder Reddy

*Department of Radiology and ‡Department of Chemistry, University of Pennsylvania, Philadelphia, Pennsylvania 19104; and *Department of Physics and †Department of Radiology, University of Pittsburgh Medical Center, Pittsburgh, Pennsylvania 15213*

Received April 16, 1999; revised August 26, 1999

In this work, we present the first triple quantum filtered (TQF) sodium MR images of the human knee joint *in vivo.* **A 3D TQF data set of 16 slices was obtained in 20 min using a TQF pulse sequence preencoded to a twisted projection imaging readout. Images clearly demarcate patellar cartilage and also demonstrate fluid signal suppressed by the triple quantum filter. Biexponential transverse relaxation times were calculated by fitting the TQF free induction decay to a theoretical signal expression. The average values from three healthy volunteers were $T^*_{2fall} = 9.59 \pm 0.35$ ms and $T^*_{2rise} = 0.84 \pm 0.06$ ms. Application of TQF imaging in biological tissues is discussed.** © 1999 Academic Press

Key Words: **sodium; cartilage; multiple quantum filter; MRI.**

INTRODUCTION

In the human skeletal system, cartilage performs the important function of facilitating joint movement and distributing mechanical load. Osteoarthritis (OA), a progressive disease of cartilage, can cause severe disability by impeding normal joint function. It is estimated that over 40 million people suffer from this debilitating disease in the United States alone (*1*). While therapeutic modalities exist, they are generally useful in the early stages of the disease. Early diagnosis would allow efficient therapeutic intervention to halt the progress of the disease.

The major components of the extracellular matrix of cartilage are proteoglycans (PG), collagen, and water. The early stage of OA is primarily associated with a loss of PG and changes in water content (*2, 3*). Although conventional proton MRI provides high-resolution images of cartilage, it is not sensitive to early changes in cartilage degeneration (*4*). Recently, sodium MR has been shown to be useful in measuring PG changes in cartilage (*5*). Furthermore, sodium in cartilage is under the influence of a nonisotropically or incompletely averaged quadrupolar interaction, which leads to biexponential relaxation rates and the generation of multiple quantum coherences. Several authors have studied sodium in biological tissues using multiple quantum filtered (MQF) NMR (*6–10*). MQF NMR signal is more sensitive to the macromolecular content and arrangement in the extracellular matrix. Therefore MQF sodium NMR may be used to probe the structural integrity of cartilage.

Recently, we have been able to obtain single quantum sodium images from cartilage both *in vitro* and *in vivo* (*5*) and triple quantum filtered (TQF) sodium images *in vitro* (*11*). TQF NMR can be exploited to image sodium in slow motional environments of the tissue and suppress sodium signal from fluids, thereby potentially increasing its sensitivity to the macromolecular changes in the tissue.

In this work, we demonstrate, for the first time, the feasibility of obtaining *in vivo* sodium TQF MR images of articular cartilage from the human knee. A TQF-prepared twisted projection imaging (TPI) sequence (*12*) was employed to obtain TQF sodium images of the knee joint from three normal volunteers. A standard TPI sequence (without TQF preencoding) was employed to obtain single quantum sodium MR images. Sodium images were compared with reference proton images obtained with a standard spoiled gradient-echo imaging sequence. We also determined sodium transverse relaxation times from the biexponential fit of the TQF time domain signal. Further optimizations to improve signal-to-noise ratio and image resolution are discussed.

THEORY

Jaccard *et al.* (*13*) and Pekar and Leigh (*6*) have developed the theory of how incomplete averaging of a quadrupole Hamiltonian over the relevant time scales leads to multiple quantum coherences and multiexponential relaxation for spin-3/2 nuclei. Here we briefly review some of the relevant concepts of biexponential transverse relaxation of sodium nuclei in the presence of quadrupolar interaction.

In the case of sodium ions undergoing fast isotropic motion, the quadrupolar interaction is averaged to zero and the three single quantum transitions are degenerate. Sodium nuclei exhibit biexponential relaxation rates in biological tissues: $R_f^{(1)}$ is the relaxation rate associated with the two outer transitions and $R_s^{(1)}$ is the rate for the inner transition. In the extreme narrowing condition ($\omega\tau_c \ll 1$, where τ_c is the correlation time describing isotropic motion and ω is the Larmor precession frequency) the

1090-7807/99 $30.00

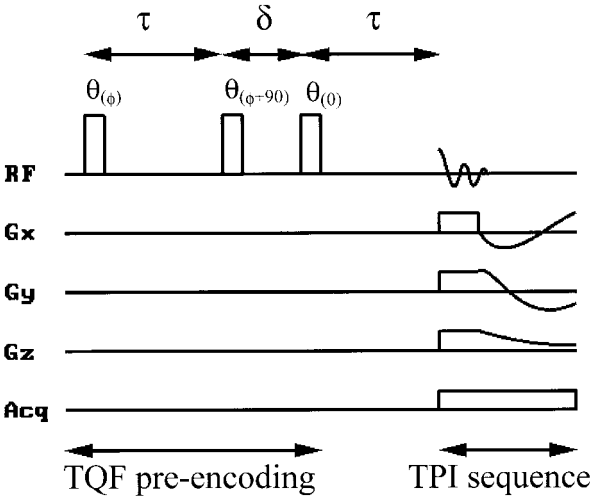

FIG. 1. Pulse sequence for triple quantum filtered magnetization prepared TPI imaging. The RF phase, ϕ, was stepped through the values: 30°, 90°, 150°, 210°, 270°, and 330°. Preparation time, τ, was set to $\tau_{optimal}$ (Eq. [4]) for each subject. The evolution time, δ, was fixed at 400 μs.

two decay rates are equal. The correlation time reflects the rotational motion modified by the chemical exchange that the sodium ions experience in cartilage. But if the motion is slow ($\omega\tau_c \geq 1$), as is the case of sodium nuclei in the presence of large PG and collagen macromolecules in cartilage, the two rates will be different. In this regime, NMR relaxation creates multiple quantum coherences that can be detected by using the appropriate multiple quantum filter (*6, 14*). Triple quantum filtered NMR provides information about sodium in cartilage undergoing slow motions.

The TQF signal intensity for a single spin-3/2 system as a function of preparation time (τ) and detection time (t) is given by (*10, 11, 13, 15*)

$$S(\tau, t) \propto (e^{-R_f^{(1)}\tau}\cos(\omega_q\tau) - e^{-R_s^{(1)}\tau}) \times (e^{-R_f^{(1)}t}\cos(\omega_q t) - e^{-R_s^{(1)}t})e^{-R_1^{(3)}\delta}. \quad [1]$$

In Eq. [1], $R_f^{(1)}$ and $R_s^{(1)}$ are the fast and slow components of the transverse relaxation rate, respectively. The relative contribution of $R_1^{(3)}$, the triple quantum coherence relaxation rate, is kept small by choosing a very short evolution time (δ). The quadrupolar interaction frequency, ω_q, is (*10, 11*)

$$\omega_q = \omega_q^l \frac{(3\cos^2\theta_{ld} - 1)}{2}, \quad [2]$$

where ω_q^l is the quadrupolar coupling constant in the local director frame and θ_{ld} is the angle between the local director and the static magnetic field (B_0).

Equation [1] shows that the quadrupolar interaction frequency affects the fast relaxation component of the NMR signal. Therefore, to compute relaxation rates accurately, one must determine ω_q in cartilage. This poses an intractable problem during *in vivo* imaging. Cartilage, like most biological tissues, is heterogeneous in nature and therefore the orientation of the local directors can assume different values. This is also true if the entire cartilage is molecularly homogeneous. The net result is an unknown distribution of ω_q values for a given sample of cartilage. In order to overcome this problem, we assume transverse relaxation rates, R_{2rise} and R_{2fall}, which are the residual quadrupolar interaction weighted $R_f^{(1)}$ and $R_s^{(1)}$ rates, respectively (*16*). Therefore, for a small evolution time (δ), Eq. [1] can be simplified to

$$S(\tau, t) \propto (e^{-R_{2rise}\tau} - e^{-R_{2fall}\tau})(e^{-R_{2rise}t} - e^{-R_{2fall}t}). \quad [3]$$

From Eq. [3], one can deduce that there will be a value of preparation time (τ) for which a maximum signal amplitude

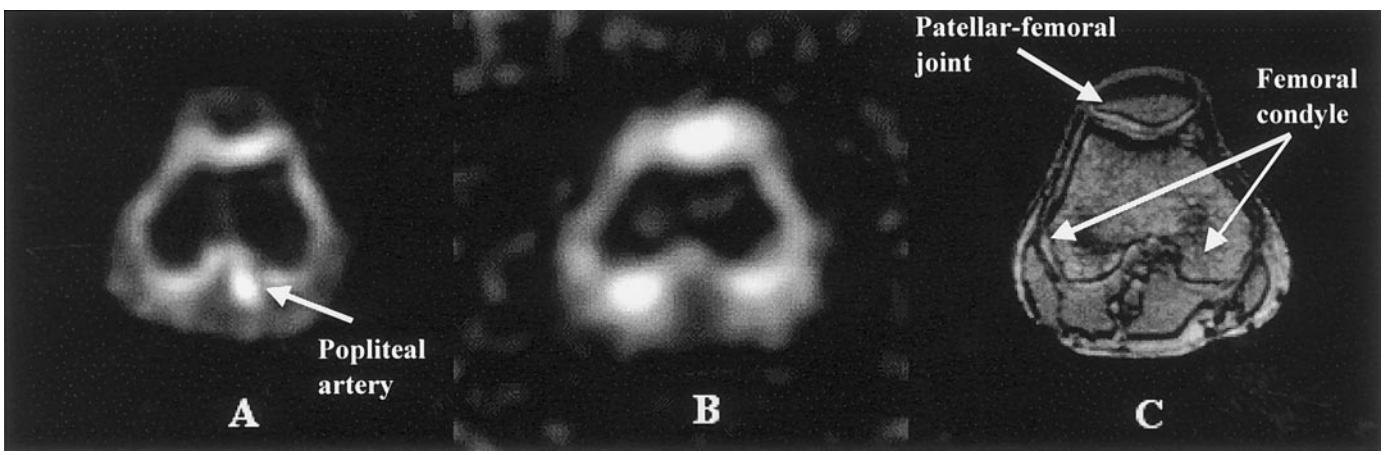

FIG. 2. *In vivo* sodium (A) single quantum and (B) TQF axial MR images across the human knee of a healthy 27-year-old male volunteer. C is the corresponding proton image of the same location. In the single quantum image (A), the arrow indicates an artery, which is not visible in the TQF image (B).

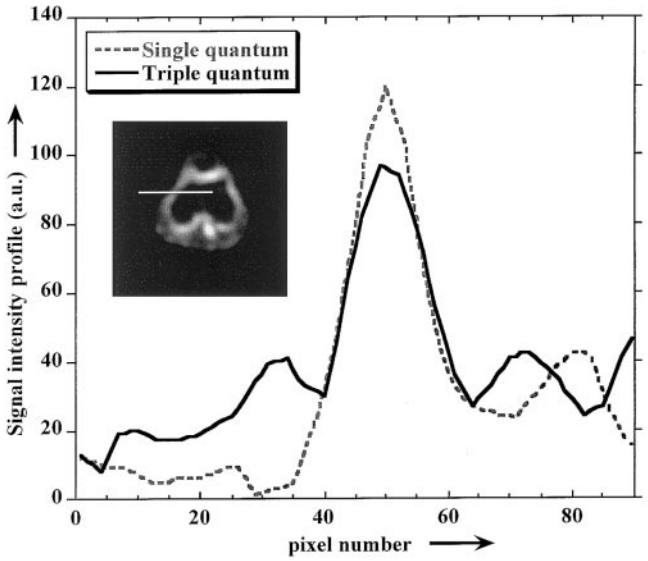

FIG. 3. Intensity profile of sodium images along a line through the femoral condyle cartilage (shown on the image) shown in Figs. 2A and 2B. SNR was 16 for single quantum images (NEX = 4) and the 8 for triple quantum images (NEX = 7).

will occur. During imaging, we set the value of τ to this optimum evolution time ($\tau_{optimal}$) which can be determined from the relaxation rates (*11*) according to the equation

$$\tau_{optimal} = \frac{\ln(R_{2rise}/R_{2fall})}{R_{2rise} - R_{2fall}}. \quad [4]$$

In our experiment, we calculated the relaxation rates by acquiring a TQF FID for an arbitrary preparation time. We then calculated the $\tau_{optimal}$ to be used during imaging. Since we calculated the relaxation times from the FID, we actually obtained R^*_{2rise} and R^*_{2fall}, the relaxation rates in the presence of inhomogeneity.

METHODS

All data acquisitions were performed on a 3.0-T whole-body scanner equipped with broad band circuitry (General Electric Medical Systems, Milwaukee, WI). A dual-tuned (^{1}H-^{23}Na), dual quadrature, 16-pole, 24-cm inner diameter birdcage coil (*17*) was used to transmit and receive.

We imaged three normal volunteers' knees using a three-pulse TQF magnetization prepared (Fig. 1) twisted projection imaging sequence (*18*). The typical length of the hard RF pulses was 500 μs. Before imaging, the optimal preparation time ($\tau_{optimal}$) was calculated in the following way. A TQF FID was obtained for an arbitrary preparation time, τ. The FID was fit to Eq. [3] to determine R^*_{2rise} and R^*_{2fall}, the transverse relaxation rates in the presence of inhomogeneities. These relaxation rates were then used in Eq. [4] to determine $\tau_{optimal}$. Single quantum sodium images were obtained by turning off the TQF pulses and using only the TPI segment of the pulse sequence. In this case, the effective delay time between excitation and detection was 400 μs. We also collected proton images using an SPGR sequence for comparison.

In the TPI sequence, the coverage of *k*-space starts at the center, moving along a radial line on the surface of concentric cones up to a fraction p ($p < 1$) of K_{max}, the largest spatial frequency value used in image reconstruction. At this point, the trajectory evolution is such that the sample density is maintained until K_{max} is reached. The two main advantages of this sequence are that (1) it provides high SNR (due to near uniform sample density throughout *k*-space) and (2) it covers *k*-space with a smaller number of projections than projection reconstruction for the same resolution. Therefore, TPI requires reduced experiment time compared to conventional projection reconstruction. Furthermore, the TPI sequence allows the use of different echo times. The signal at the center of *k*-space is directly related to the average intensity of the image. Therefore a very short TE will lead to poor SNR since the TQF signal is zero at $t = 0$ and reaches a maximum at $t \sim 3$ ms. The acquisition of the signal starts at the center of *k*-space and therefore the echo time (TE) was chosen to coincide with the maximum of the TQF signal (which occurs at $\tau_{optimal}$). The evolution time of (δ) was kept as short as possible (400 μs). In order to obtain the maximum TQF signal, the preparation time (τ) was also set to $\tau_{optimal}$. The FOV was 20 × 20 cm, resulting in a voxel volume of 0.5 cc. TE/TR = 3.2/100 ms and seven averages were used. Total TQF imaging time for each 3D data set was ~20 min. Sodium single quantum images were obtained with the following imaging parameters: FOV was 20 × 20 cm, with a voxel volume of 0.06 cc. TE/TR = 0.4/100 ms and four averages were used. Total imaging time for each 3D data set was ~10 min.

Proton MRI was performed, using the same coil, immediately following sodium imaging. We used a spoiled gradient-

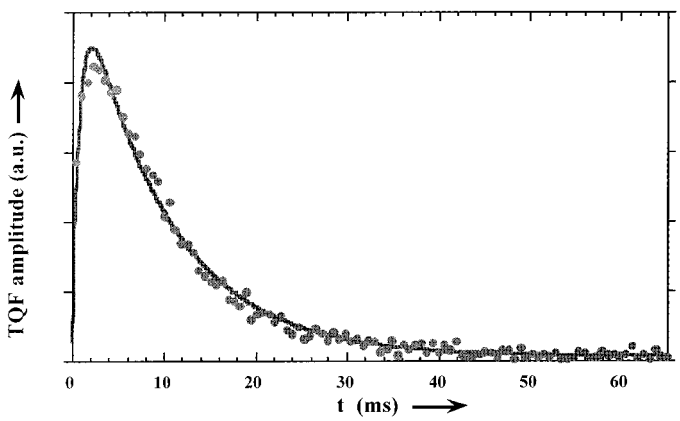

FIG. 4. Sodium TQF free induction decay signal (●) and fit (—) from the knee of the same subject shown in Fig. 2. Biexponential fit resulted in transverse relaxation times T^*_{2fall} = 10 ms and T^*_{2rise} = 0.93 ms.

echo sequence with TE/TR = 8/40 ms, FOV = 20 × 20 cm, 1.5-mm-thick slices with pixel dimensions of 256 × 192.

To correct for B_1 inhomogeneity, we constructed B_1 maps prior to the experiments. We computed these maps from a set of lower resolution sodium images by varying the RF amplitude (A) and then using a pixel-by-pixel fit of the signal intensity ($I(x,y,z;A)$) to A (*18*):

$$I(x,y,z;A) = I_0(x,y,z) + \rho'(x,y,z)\sin(hB_1(x,y,z)A), \quad [5]$$

where h is a constant, $\rho'(x,y,z)$ is the apparent spin density of the low-resolution scans, and $I_0(x,y,z)$ is a baseline term used to reduce the bias induced by noise in the data. Once the excitation field was determined, the single quantum and triple quantum sodium images could be corrected for B_1 inhomogeneity by dividing them by the correction factor

$$\Xi(x,y,z) = B_1(x,y,z)\sin^5(B_1(x,y,z)\xi), \quad [6]$$

where ξ is a scale factor obtained by adding the spin density times the correction factor in Eq. [6] over the entire imaged volume and retaining the ξ which maximized that sum. This process simulates the way in which the tip angle for the actual acquisition was selected (by maximizing the triple quantum signal over the whole volume).

RESULTS AND DISCUSSION

Figure 2 shows a sodium single quantum (A) and TQF (B) MR image of the same axial slice from the patellar–femoral joint of a healthy 27-year-old male volunteer. Note that the bright artery at the bottom of image A (indicated by arrow) is not visible in the TQF image. This is because the TQF sequence suppresses signal from the motionally narrowed sodium in blood. Although the concentration of sodium is lower in blood than in cartilage, the T_2 of sodium in blood is longer and therefore results in an enhanced signal from the artery in the single quantum image. Thus the signal from the artery served as an internal control for evaluating the filtering capability of the TQF sequence. Figure 2C is the corresponding proton image of the same axial slice shown for comparison.

Figure 3 shows a profile of sodium signal intensity across the articular cartilage in the femoral condyle region of Figs. 2A and 2B. The SNR of the single quantum sodium images was 16 (NEX = 4), whereas that for the TQF images was 8 (NEX = 7). The lower SNR for TQF images is expected because a smaller fraction of sodium contributes to the signal. The TQF signal is more sensitive to sodium in cartilage than in the surrounding tissues. Therefore TQF images are devoid of any signal from the surrounding tissues. This property can be exploited in separating cartilage signal from fluid signal in subjects with enhanced synovial fluid.

Figure 4 is a plot of the TQF FID obtained from the same individual for a preparation time of 2.4 ms. By fitting the envelope of the FID to a biexponential equation (Eq. [3]), the average transverse relaxation times were (for $n = 3$) $T^*_{2\text{fall}} = 9.59 \pm 0.35$ ms and $T^*_{2\text{rise}} = 0.84 \pm 0.06$ ms.

It is possible to further improve SNR and resolution of these images by reducing the coil size and shortening the pulse lengths. To this end, we are in the process of building a dedicated coil for knee imaging. We are also in the process of implementing the sequence at a higher field (4 T) and employing stronger gradients to further improve image quality. It is possible to apply this technique to image other biological tissues as well.

CONCLUSIONS

We have demonstrated for the first time that it is feasible to obtain TQF sodium images of cartilage *in vivo* in a reasonable time. We have also measured the transverse relaxation times *in vivo*. While single quantum images can be used to determine PG content, TQF images are more specific because they show sodium in slow motion regime primarily associated with the presence of macromolecules. The images may potentially be sensitive to structural changes in macromolecule arrangement in the extracellular matrix. Furthermore, TQF imaging can be used to suppress unwanted fluid signals.

ACKNOWLEDGMENTS

This work was performed with the help of an NIH-supported resource center (NIH RR02305), NIH Grants RO1-AR45242 and RO1-AR45404, and the Whitaker Foundation. The authors thank Sridhar Charagundla for useful discussions. We thank Professors Felix W. Wehrli and John S. Leigh for their encouragement and support.

REFERENCES

1. R. S. Fife, A short history of osteoarthritis, *in* "Osteoarthritis: Diagnosis and Medical/Surgical Management" (R. W. Moskowitz, H. S. Howell, V. M. Goldberg, and H. J. Mankin, Eds.), p. 11, Saunders, Philadelphia (1992).
2. H. J. Mankin, H. Dorfman, and L. Zarins, Biochemical and metabolic abnormalities in articular cartilage from osteoarthritic human hips II. Correlation of morphology with biochemical and metabolic data, *J. Bone Joint Surg.* **53A,** 523–537 (1971).
3. A. A. van de Loo, O. J. Arntz, I. G. Otterness, and W. B. van den Berg, Proteoglycan loss and subsequent replenishment in articular cartilage after a mild arthritic insult by IL-1 in mice: Impaired proteoglycan turnover in the recovery phase, *Agents Actions* **41,** 200–208 (1994).
4. M. P. Recht and D. Resnick, MR imaging of articular cartilage: Current status and future directions, **163,** 283–290 (1994).
5. R. Reddy, E. K. Insko, E. A. Noyszewski, R. Dandora, J. B. Kneeland, and J. S. Leigh, Sodium MRI of human articular cartilage in vivo, *Magn. Reson. Med.* **39,** 697–701 (1998).
6. J. Pekar and J. S. Leigh, Detection of bi-exponential relaxation in

sodium-23 facilitated by double quantum filtering, *J. Magn. Reson.* **69,** 582–584 (1986).

7. W. D. Rooney and C. S. Springer, Jr., A comprehensive approach to the analysis and interpretation of the resonances of spins 3/2 from living systems, *NMR Biomed.* **4,** 209–226 (1991).
8. W. D. Rooney and C. S. Springer, Jr., The molecular environment of intracellular sodium: ^{23}Na NMR relaxation, *NMR Biomed.* **4,** 227–245 (1991).
9. C. S. Springer, Biological systems: Spin-3/2 nuclei, *in* "Encyclopedia of Nuclear Magnetic Resonance" (D. M. Grant and R. K. Harris, Eds.), p. 940–951, Wiley, New York (1996).
10. R. Reddy, S. C. Li, E. A. Noyszewski, J. B. Kneeland, and J. S. Leigh, In vivo sodium multiple quantum spectroscopy of human articular cartilage, *Magn. Reson. Med.* **38,** 207–214 (1997).
11. R. Reddy, E. K. Insko, and J. S. Leigh, Triple quantum sodium imaging of articular cartilage, *Magn. Reson. Med.* **38,** 279–284 (1997).
12. F. E. Boada, J. S. Gillen, G. X. Shen, S. Y. Chang, and K. R. Thulborn, Fast three dimensional sodium imaging, *Magn. Reson. Med.* **37,** 706–715 (1997).
13. G. Jaccard, S. Wimperis, and G. Bodenhausen, Multiple quantum NMR spectroscopy of S = 3/2 spins in isotropic phase: A new probe for multiexponential relaxation, *J. Chem. Phys.* **85,** 6282–6293 (1986).
14. P. S. Hubbard, Non exponential nuclear magnetic relaxation by quadrupolar interactions, *J. Chem. Phys.* **53,** 985–987 (1970).
15. U. Eliav and G. Navon, Analysis of double-quantum-filtered NMR spectra of ^{23}Na in biological tissues, *J. Magn. Reson. B* **103,** 19–29 (1994).
16. U. Eliav and G. Navon, Quadrupole-echo techniques in multiple-quantum-filtered NMR spectroscopy of heterogeneous systems, *J. Magn. Reson. A* **115,** 241–253 (1995).
17. G. X. Shen, F. E. Boada, and K. R. Thulborn, Dual-frequency, dual quadrature, birdcage RF coil design with identical B1 pattern for sodium and proton imaging of the human brain at 1.5 T, *Magn. Reson. Med.* **38,** 717–725 (1997).
18. F. E. Boada, J. Gillen, D. C. Noll, G. X. Shen, and K. R. Thulborn. Data acquisition and post-processing strategies for fast quantitative sodium imaging, *Int. J. Imag. Syst. Tech.* **8,** 544–550 (1997).